Flux tubes in three-dimensional lattice gauge theories

Howard D. Trottier

Department of Physics, Simon Fraser University, Burnaby, British Columbia, Canada V5A 1S6*
and TRIUMF, 4004 Wesbrook Mall, Vancouver, British Columbia, Canada V6T 2A3

R. M. Woloshyn

TRIUMF, 4004 Wesbrook Mall, Vancouver, British Columbia, Canada V6T 2A3

Measurements of flux tubes generated by sources in different representations of SU(2) and U(1) lattice gauge theory in three dimensions are reported. Heavy "quarks" are considered in three representations of SU(2): fundamental ($j = 1/2$), adjoint ($j = 1$), and quartet ($j = 3/2$). Wilson loops are used to introduce a static quark-antiquark ($Q_j\overline{Q}_j$) pair. Several attributes of the fields generated by the $Q_j\overline{Q}_j$ pair are measured. In particular, the first direct lattice measurements of the flux-tube cross section $\mathcal{A}_j$ as a function of representation are made. It is found that $\mathcal{A}_j \approx$ const, to within about 10% (a rough estimate of the overall quality of the data). The results are consistent with a connection between the string tension σ_j and cross section suggested by a simplified model of flux-tube formation, $\sigma_j = g^2 j(j + 1)/(2\mathcal{A}_j)$ [where g is the gauge coupling], given that the string tension scales like the Casimir eigenvalue $j(j + 1)$, as observed in previous lattice studies in both three and four dimensions (and confirmed here up to the quartet representation). These results can be used to discriminate among phenomenological models of the physics underlying confinement. Flux-tube measurements are also made in compact three-dimensional QED, which exhibits electric confinement due to magnetic monopole condensation. Singly and doubly charged Wilson loops are considered. The string tension is found to scale like the squared charge, and the flux-tube cross section is found is be independent of the charge, to a good approximation. The results of these three-dimensional SU(2) and U(1) simulations taken together lend some support, albeit indirectly, to a conjecture that the dual superconductor mechanism underlies confinement in compact gauge theories in both three and four dimensions.

PACS number(s): 12.38.Gc, 11.15.Ha, 12.38.Aw, 12.40.Aa

I. INTRODUCTION

Flux-tube formation provides an attractive description of confinement in quantum chromodynamics (QCD). In a simplified flux-tube picture of a very heavy quark-antiquark pair, color-electric field lines running between the quarks are assumed to be "squeezed" into a cylinder whose cross section is independent of the quark separation R (ignoring end effects), resulting in linear confinement.

Consider heavy "quarks" in an arbitrary representation of the gauge group, which we take to be SU(2) for convenience. The color-electric field E_j between quarks in the jth representation is determined, in an Abelian approximation, by Gauss' law [1] $E_j\mathcal{A}_j = gQ_j$, where the quark color "charge" Q_j is related to the group Casimir eigenvalue $Q_j^2 = j(j + 1)$, g is the gauge coupling, and $\mathcal{A}_j$ is the cross section of the flux tube. In this simplified model, E_j is assumed to be constant across the flux-tube cross section. In the case of nonfundamental representation sources, R is also assumed to be below the threshold for fission of the tube. The interaction energy of the system $V_j^{\mathrm{int}}(R) = \frac{1}{2}E_j^2\mathcal{A}_jR = \sigma_jR$, and thus the string tension σ_j is given by

$$\sigma_j = \frac{g^2 j(j + 1)}{2\mathcal{A}_j}. \tag{1}$$

In a more detailed flux-tube model, the color field E_j may vary in magnitude across the flux-tube cross section; the cross section in Eq. (1) is then defined by $\mathcal{A}_j \equiv (\int E_j dA_j)^2 / \int E_j^2 dA_j$; it is also possible to relax the constraint that $\mathcal{A}_j$ be independent of R.

If the general features of the flux-tube model of confinement are consistent with QCD, then the connection Eq. (1) between σ_j and $\mathcal{A}_j$ should hold. However, within the context of the flux-tube picture, $\mathcal{A}_j$ is an unknown function of the quark representation. The cross section is determined by the fundamental dynamics of QCD. Flux-tube formation has been observed in lattice QCD simulations in four dimensions [2–7] and as well as in three dimensions [8]. However, previous flux-tube measurements have only been made for fundamental representation sources.

This paper presents results of the first direct lattice measurements of $\mathcal{A}_j$ for static quarks in different representations of the gauge group. This work is aimed in part at establishing the connection Eq. (1) between the string tension and flux-tube cross section. As well, the results obtained here go beyond the flux-tube model, providing

---

* Permanent address.

     <u>48</u>   2290

important new information about the dynamics underlying confinement.

For example, if confinement is due to a bulk property of the QCD vacuum, such as a vacuum pressure, then $\mathcal{A}_j$ is expected to increase with representation (a natural "mechanical" response of a "medium" to the injection of more intense fields). Consequently, in such a scenario, the string tension σ_j is expected to increase with representation less rapidly than the quark Casimir eigenvalue. This situation is realized in a wide class of phenomenological models, including bag models [1,9], models based on a description of the QCD vacuum as a color-dielectric medium [10], and some models of confinement based on vacuum condensation [11].

The MIT bag [9] is typical of this general class of models. In the case of the heavy quark-antiquark $(Q_j \overline{Q}_j)$ system described above, the magnitude of the color-electric field is determined by a balance between the pressure generated by the field and an external "bag" pressure B [1], $\frac{1}{2}E_j^2 = B$. It follows that $\mathcal{A}_j \propto Q_j$, and the resulting string tension σ_j also scales as the square root of the Casimir eigenvalue, $\sigma_j \propto [j(j+1)]^{1/2}$.

In fact, the phenomenological models discussed above are not compatible with lattice simulations, which have shown that the string tension actually scales to an excellent approximation as the Casimir eigenvalue of the representation. This has been observed for both SU(2) and SU(3) gauge groups [12]. In the context of the flux-tube model, this suggests that the cross section $\mathcal{A}_j$ is *independent* of representation.

Direct measurements of the flux-tube cross section for heavy quark-antiquark $(Q_j \overline{Q}_j)$ sources are obtained here in three representations of three-dimensional SU(2) lattice-gauge theory: fundamental $(j = 1/2)$, adjoint $(j = 1)$, and quartet $(j = 3/2)$. A more thorough check of scaling and finite-volume effects is achieved by working in three dimensions than would be obtained (with the same computing power) in four dimensions. We think that our results are relevant to the problem of confinement in four-dimensional QCD. In particular, previous lattice studies have shown that the string tension scales like the Casimir eigenvalue of the representation in three dimensions [13, 14], as well as in four dimensions [12]. Moreover, the flux tube picture of confinement is qualitatively the same in both three and four dimensions. It is therefore reasonable to expect that the qualitative features of flux tubes reported here would be reproduced in four dimensions. Of course, such a calculation can and should be done.

We find $\mathcal{A}_j \approx$ const for the three representations, to within about 10% (a rough estimate of the overall quality of our data). This is consistent with the flux-tube picture, given that the string tension scales like the Casimir eigenvalue of the representation (which is confirmed here up to the quartet representation). Several additional qualitative features of the flux-tube picture are also verified.

These results suggest a connection between confinement in QCD and the physics of a dual superconductor [15]. It is well known that dual-superconductivity (magnetic-monopole condensation) results in confinement of electric charges in compact QED in three dimensions (QED₃) [16]. A simple extension of the analytical calculation of Ref. [17] in the Villain approximation to the Wilson action, to include Wilson loops for multiply charged sources, demonstrates that the string tension scales like the squared charge.

We have performed lattice simulations of singly and doubly charged Wilson loops in compact QED₃, and our results confirm the expected scaling properties of the string tension and flux-tube cross section. The potential is found to scale like the squared charge to within a few percent, and the flux tubes in the two cases have the same cross section to within about 10%. The results of our three-dimensional SU(2) and U(1) simulations taken together lend some support, albeit indirectly, to the dual-superconductor picture of confinement in four-dimensional QCD [18].

II. METHOD

To begin with, we consider the three-dimensional SU(2) lattice theory. Wilson loops are used to introduce static $Q_j \overline{Q}_j$ sources. Lattice measurements of the color-electric and -magnetic fields generated by these sources are obtained from correlators $\mathcal{F}_j^{\mu\nu}$ of plaquettes with a Wilson loop,

$$\mathcal{F}_j^{\mu\nu}(x) \equiv -\frac{\beta}{a^3}\left[\frac{\langle W_j \frac{1}{2}\mathrm{Tr}\, U^{\mu\nu}(x)\rangle}{\langle W_j\rangle} - \langle \frac{1}{2}\mathrm{Tr}\, U^{\mu\nu}\rangle \right], \qquad (2)$$

where $U^{\mu\nu}(x)$ is the plaquette located at x (measured relative to the center of the Wilson loop) and W_j is the normalized trace of the Wilson loop in the jth representation:

$$W_j \equiv \frac{1}{2j+1}\mathrm{Tr}\left\{ \prod_{l \in L} \mathcal{D}_j[U_l] \right\}. \qquad (3)$$

$\mathcal{D}_j[U_l]$ denotes an appropriate irreducible representation of the link U_l, and L the closed loop. $\beta \equiv 4/(g^2 a)$, where the coupling constant g has dimensions of $(\mathrm{mass})^{1/2}$ in three dimensions.

In the continuum limit, the trace of a 1×1 plaquette is by construction independent of representation (up to overall normalizations). As in several previous lattice calculations of higher-representation Wilson loops (cf. Refs. [12–14]), we use the action expressed in terms of links in the fundamental representation to perform simulations at arbitrary β. The trace of the plaquette $U^{\mu\nu}$ in the fundamental representation is also used to compute the correlators of Eq. (2).

In the continuum limit the correlator $\mathcal{F}_j^{\mu\nu}$ corresponds to the expectation value of the square of the Euclidean field strength $F^{a\mu\nu} = \partial^\mu A^{a\nu} - \partial^\nu A^{a\mu} + g\epsilon^{abc}A^{b\mu}A^{c\nu}$:

$$\lim_{\beta\to\infty}\mathcal{F}_j^{\mu\nu} = \frac{1}{2}\left\langle \sum_a (F^{a\mu\nu})^2 \right\rangle_{Q_j\overline{Q}_j} - \frac{1}{2}\left\langle \sum_a (F^{a\mu\nu})^2 \right\rangle_0,$$

$$(4)$$

where the expectation value $\langle \cdots \rangle_{Q_j \overline{Q}_j}$ is taken in a state with external sources in the jth representation and $\langle \cdots \rangle_0$ is the vacuum expectation value.

To compute the energy density, the Euclidean three-axis is identified with a temporal side of the Wilson loop and the one-axis with a radial side. We separate contributions to the total-energy density $\mathcal{E}_{\rm tot}$ corresponding to the two spatial components of the color-electric field (in the directions parallel and perpendicular to the line joining the quarks) and the color-magnetic field (a scalar in three dimensions):

$$\mathcal{E}_j^{\rm tot}(x) = \mathcal{E}_j^{\parallel}(x) + \mathcal{E}_j^{\perp}(x) + \mathcal{E}_j^B(x), \qquad (5)$$

where

$$\mathcal{E}_j^{\parallel}(x) \equiv -\mathcal{F}_j^{13}(x),$$

$$\mathcal{E}_j^{\perp}(x) \equiv -\mathcal{F}_j^{23}(x), \qquad (6)$$

$$\mathcal{E}_j^B(x) \equiv \mathcal{F}_j^{12}(x).$$

Note the relative minus sign between the electric and magnetic components of the Euclidean energy density.

Previous flux measurements for fundamental representation sources have been made in four dimensions [2–7] and in three dimensions [8]. Following Haymaker and Wosiek [5], we achieve a significant enhancement in the signal to noise for the correlators by replacing Eq. (2) with

$$\mathcal{F}_j^{\mu\nu}(x) \approx -\frac{\beta}{a^3} \left[\frac{\langle W_j \frac{1}{2} \mathrm{Tr}\, \{U^{\mu\nu}(x) - U^{\mu\nu}(x_R)\} \rangle}{\langle W_j \rangle} \right], \qquad (7)$$

where x_R is a reference point chosen far enough from the Wilson loop that the factorization $\langle W_j U(x_R) \rangle \simeq \langle W_j \rangle \langle U \rangle$ is satisfied. As in Ref. [5], we find that this happens well within the lattice volume. We verified explicitly that the right-hand side of Eq. (7) is insensitive, within our statistical errors, to variations in x_R over a wide range (when measurements are made for x in a region around the Wilson loop of sufficient size to suit our purposes). The results presented here were obtained with x_R taken at a distance of half the lattice size from the center of the Wilson loop, in the direction transverse to the plane of the loop. The advantage to using Eq. (7) is that the fluctuations in the product $W_j U^{\mu\nu}$, due mainly to the Wilson loop, tend to cancel in the vacuum subtraction when computed configuration by configuration.

Another reduction in the statistical errors is readily achieved by performing some link integrations analytically, following the multihit procedure introduced by Parisi, Petronzio, and Rapuano [19]. Consider a link variable U_l which appears linearly in the observable of interest. The simplest analytical integration over U_l takes account of nearest-neighbor couplings in the action

$$\int [dU_l] \mathcal{D}_j[U_l] e^{\beta \mathrm{Tr}(U_l K_l^\dagger)/2}$$

$$= \frac{I_{2j+1}(\beta k_l)}{I_1(\beta k_l)} \mathcal{D}_j[V_l] \int [dU_l] e^{\beta \mathrm{Tr}(U_l K_l^\dagger)/2}, \qquad (8)$$

where K_l is the sum of the four "staples" coupling to the link of interest U_l and

$$k_l V_l \equiv K_l, \quad \det V_l = 1. \qquad (9)$$

A further variance reduction has been developed by Mawhinney [14], which takes account of effective next-to-nearest-neighbor interactions with the link of interest:[1]

$$\int [dU_l] \mathcal{D}_j[U_l] e^{-\beta S}$$

$$= \frac{I_{2j+1}(\beta k_l')}{I_1(\beta k_l')} \frac{I_{2j+1}(\beta k_l)}{I_1(\beta k_l)} \mathcal{D}_j[V_l' V_l] \int [dU_l] e^{-\beta S}, \qquad (10)$$

where S is the action [only next-to-nearest-neighbor couplings to U_l are relevant in Eq. (10)] and

$$k_l' V_l' \equiv \sum_{\hat{l}_\perp} U_{\hat{l}_\perp}(x) \sum_{\hat{\mu} \neq \hat{l}_\perp} U_{l\hat{\mu}}(x + \hat{l}_\perp) U_{\hat{l}_\perp}^\dagger(x),$$

$$\det V_l' \equiv 1. \qquad (11)$$

$\hat{l}_\perp$ are four unit vectors perpendicular to $\hat{l}$. The oriented plaquette $U_{l\hat{\mu}}(x + \hat{l}_\perp)$ is computed with the link $U_l(x + \hat{l}_\perp)$ appearing first on the left [x is the position of the base of the link U_l in Eq. (10)]. The sum over unit vectors $\hat{l}_\perp$ and $\hat{\mu}$ in Eq. (11) is taken over both parallel and antiparallel orientations with respect to a set of fixed basis vectors. An integration over the four links $U_l(x + \hat{l}_\perp)$ is implicit in Eq. (10).

The second-order variance reduction of Eq. (10) cannot be applied to the links in the corners of the Wilson loop, since some links would then appear more than once in the integrand. Likewise, the first-order variance reduction Eq. (8) can only be applied to one link in a corner. Further restrictions apply to calculations of the plaquette correlators.

For Wilson loops with less than six links on a side, we use the first-order variance reduction Eq. (8) for all links in the loop, except for one link at each corner, where no variance reduction is used. A plaquette correlator can be measured simultaneously provided that all sides of the plaquette are at least one node from the sides of the Wilson loop.

For Wilson loops of size 6×6 or larger, we minimize the variance by using a combination of first- and second-order variance reductions. Equation (8) is applied to the

---

[1] Mawhinney derived next-to-nearest-neighbor variance reductions for fundamental and adjoint representations by employing an axial-gauge fixing [14]. We have generalized his result to arbitrary representations without gauge fixing.

first link and to the second-to-last link on each (oriented) side of the Wilson loop; Eq. (10) is applied to all other links, except the last link on each side, where no variance reduction is used. In this case, a correlator can be measured simultaneously only if all sides of the plaquette are at least two nodes from the sides of the Wilson loop. [This variance-reduction scheme can also be applied to Wilson loops as small as 4×4 if measurements of correlators near the center of the loop are not desired. This scheme is significantly more effective than the one employed in Ref. [14], which uses only second-order variance reductions.]

For large β, $k_l \sim 4$ and $k_l' \sim 12$; Eq. (10) then provides an estimate of the reduction v_{red} in the variance of a Wilson loop using the above scheme, compared to the variance when only "unreduced" links are used (cf. Refs. [20, 14])

$$v_{\mathrm{red}} \approx \left(\frac{I_{2j+1}(12\beta)}{I_1(12\beta)} \right)^{(2T+2R-12)} \left(\frac{I_{2j+1}(4\beta)}{I_1(4\beta)} \right)^{(2T+2R-4)} .$$

(12)

For example, the variance reduction for a Wilson loop of size 6×6 in the quartet representation at $\beta = 10$ is estimated to be a factor of ≈ 90. Our numerical results are consistent with Eq. (12).

The trace of an element of the group in the jth representation can be expressed in terms of its trace in the fundamental representation using trigonometric relations among the group characters. In the case of the adjoint and quartet representations [21],

$$W_{3/2} = 2W_{1/2}^3 - W_{1/2},$$

(13)

$$W_1 = \left(4W_{1/2}^2 - 1 \right) \Big/ 3.$$

Hence one need only compute the Wilson loop in the fundamental representation, using the "unreduced" links U_l, or the "reduced" elements V_l, V_l' of Eqs. (8) and (10), as the case may be. The Wilson loops in higher representations then follow from Eq. (13). The Bessel functions for the analytical integrations are tabulated separately for the three representations.

III. RESULTS AND DISCUSSION

Our main results were obtained on a 32^3 lattice at $\beta = 10$ (which is well within the scaling region for the string tension on a lattice of this size [14]). Wilson loops and plaquette correlators were calculated in the three representations $j = 1/2$, 1, and 3/2 for all loops of sizes $T \times R$ from 3×4 to 8×8 (these observables were measured in groups in several separate runs). Some additional data was taken at $\beta = 14$ in order to check for scaling of the physical flux-tube dimensions. A standard heat-bath algorithm was employed. More than 10 000 sweeps were typically used for thermalization. 2 000 measurements were made, taking 20 sweeps between measurements. The resulting integrated autocorrelation times τ_{int} for the Wilson loops generally satisfy $\tau_{\mathrm{int}} \lesssim 0.5$, consistent with the results of a systematic study made in Ref. [14]. Es-

timates of the statistical errors were obtained using the jackknife method. However, measurements of different observables (and of a given observable in the three representations) tend to be strongly correlated, since many Wilson loops and plaquette correlators were measured simultaneously on a given lattice.

The quartet representation is much more difficult to measure than the two lower representations, due to the exponential suppression of the Wilson loop with the $Q_j \overline{Q}_j$ potential, which is found to scale with the Casimir eigenvalue of the representation. Energy-density measurements in the quartet case obtained from loops larger than about 6×6 are of poor quality, although these data are consistent with conclusions drawn from results obtained from smaller loops.

Representative data for Wilson loops in the three representations are shown in Fig. 1. Earlier studies have shown that the potentials scale with the Casimir eigenvalue of the representation at essentially all lengths scales R [13, 14]. This is made evident in Fig. 1, where the logarithms of the Wilson loops are scaled by a ratio of Casimirs eigenvalues:

$$c_j \equiv \frac{3/4}{j(j+1)}.$$

(14)

The quantity $-\ln\langle W_j(T, R)\rangle/T$, which extrapolates to the $Q_j \overline{Q}_j$ potential $V_j(R)$ in the limit $T \to \infty$, is found to scale as $j(j+1)$ to within a few tenths of a percent at all T and R considered here. A simple extrapolation of the data using $V_j(R) \approx \ln[\langle W_j(T_{\mathrm{max}}-1, R)\rangle/\langle W_j(T_{\mathrm{max}}, R)\rangle]$, where T_{max} is the largest T value in the data set, gives agreement to a few tenths of a percent with the results of a careful statistical analysis of fundamental and adjoint Wilson loops reported in Ref. [14].

Several attributes of the plaquette correlators were measured. To begin with, results for the fundamental and adjoint representations are presented. The correlators were measured over a range of distances $x_\perp$ from the center of the Wilson loop, in the direction normal to the plane of the loop. Results for the $T \times R = 8 \times 6$ loop are shown in Fig. 2. The cross sections of the fundamental
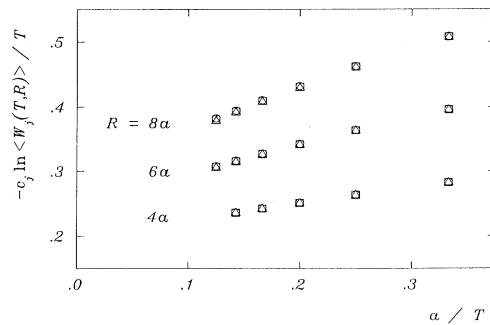

FIG. 1. T evolution of Wilson loops in three representations of SU(2) lattice-gauge theory: $j = 1/2$ ($\circ$), $j = 1$ ($\square$), and $j = 3/2$ ($\triangle$). c_j is a ratio of Casimir eigenvalues, defined in Eq. (14). The quantity $-\ln\langle W_j(T, R)\rangle/T$ extrapolates to the $Q_j \overline{Q}_j$ potential in the limit $T \to \infty$.

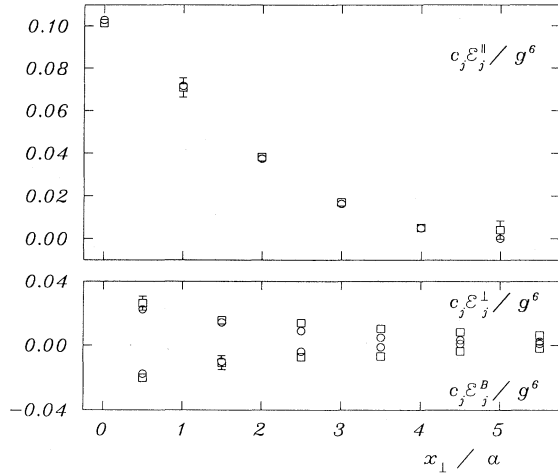FIG. 2. Energy-density profiles transverse to the plane of the $T \times R = 8 \times 6$ Wilson loop [$j = 1/2$ (o), $j = 1$ (□)]. These results are an average over plaquettes with centroids at distances $\pm x_\perp$ transverse to the plane of the loop.

and adjoint representation flux tubes are indistinguishable within statistical errors. This is true for all Wilson loops that were considered. For example, the T evolution of $\mathcal{E}_j^\parallel$ for $R = 6$ Wilson loops is illustrated in Fig. 3. As observed in Refs. [4, 6], the plaquette correlators are more sensitive to higher states than the Wilson loop. Our data are consistent with a one-excited-state parametrization given in Ref. [6].

Figure 2 demonstrates that the component of the color-electric field parallel to the line joining the charges dominates the energy, as assumed in the flux-tube model. The magnetic energy turns out to be negative, which has also been observed in four-dimensional SU(2) lattice theory [5]. The formation of a well-defined flux tube is demonstrated by measurements of $\mathcal{E}_j^\parallel$ in the plane of the Wilson loop. Figure 4 shows $\mathcal{E}_j^\parallel$ for the $T \times R = 6 \times 8$ loop as a function of the longitudinal distance $x_\parallel$ of the plaquette centroid from the center of the loop. Note the approximate symmetry of the energy density about the center of
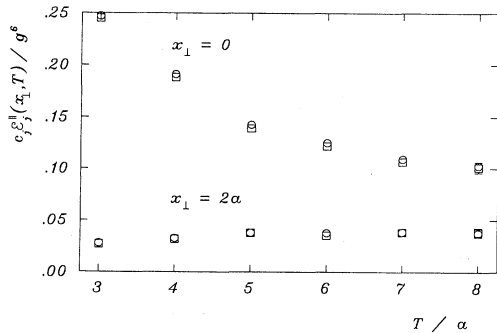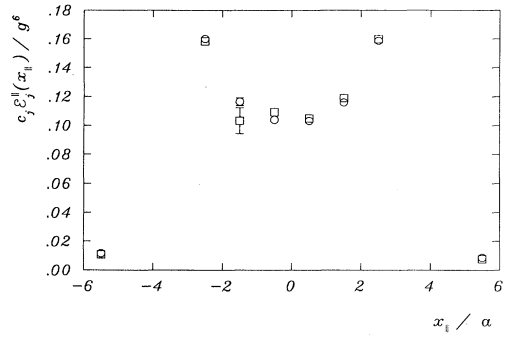

FIG. 4. Energy-density profile in the plane of the $T \times R = 6 \times 8$ Wilson loop [$j = 1/2$ (o), $j = 1$ (□)]. $x_\parallel$ is the distance of the centroid of the plaquette from the center of the Wilson loop. The radial sides of the Wilson loop are located at $x_\parallel = \pm 4a$. Plaquettes with a side touching the Wilson loop cannot be measured using the variance reduction of Eq. (8), and are not shown.

the loop. The formation of the flux tube is further illustrated in Fig. 5, where $\mathcal{E}_j^\parallel$ is shown as a function of the radial separation R of the Wilson loop (for fixed $T = 6$).

A stringent test of energy-density calculations using Eq. (7) is provided a sum rule derived by Michael [22]

$$a^2 \sum_{\vec{x}} \mathcal{E}_j^{\text{tot}}(\vec{x}) = V_j(R). \tag{15}$$

The analogous sum rule in four-dimensional SU(2) was studied in detail by Haymaker and Woseik [5]. The flux-tube picture suggests a related sum rule that is much simpler to measure. If the interaction energy is dominated by a constant color-electric field along the line joining the charges (as expected in the limit of quark separations much greater than the flux-tube thickness), then the integral of the energy density along one transverse "slice" of the flux tube should equal the string tension (cf. $\sigma_j = \lim_{R \to \infty} [V_j(R) - V_j(R - a)]/a$):

$$a \sum_{|x_\perp|} \mathcal{E}_j^\parallel (x_\perp, x_\parallel = \text{fixed}) \approx \sigma_j, \tag{16}$$

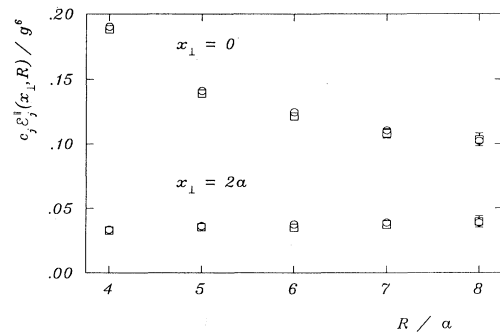FIG. 3. T evolution of $\mathcal{E}_j^\parallel (x_\perp = 0, 2a)$ for Wilson loops with $R = 6$ [$j = 1/2$ (o), $j = 1$ (□)].

FIG. 5. Energy density $\mathcal{E}_j^\parallel (x_\perp = 0, 2a)$ as a function of R, for fixed $T = 6$ [$j = 1/2$ (o), $j = 1$ (□)].

where the sum is taken over positive and negative distances $x_\perp$ from the plane of the Wilson loop.

Our results are in good agreement with Eq. (16). Figure 6 shows the left-hand side of this equation for the $T \times R = 8 \times 6$ loop in the fundamental and adjoint representations, using a variable cutoff $x_\perp^*$ on the sum. The right-hand side of Eq. (16) is illustrated by the dashed line in Fig. 6 (our estimates of the string tension in the two representations agree with Ref. [14] to within a few percent). These results again demonstrate that the flux-tube cross sections for the fundamental and adjoint representations are indistinguishable within statistical errors.

Figures 2–6 also demonstrate that the local-energy densities scale to a good approximation like the Casimir eigenvalue of the representation throughout the flux tube. This is a very strong test of the validity of the flux-tube model for $\mathcal{A}_j = $ const. Since the magnitude of the color-electric field varies across the flux-tube cross section (cf. Fig. 2), a proper determination of the numerical value of $\mathcal{A}_j$ should be made in terms of expectation values of the color field, as described below Eq. (1) [some prescription for defining the Abelian projection of the color field would also be required]. However, a rough estimate $\mathcal{A}_j \approx 8a$ inferred from Fig. 6 is consistent with Eq. (1), given the estimate of the string tension $c_j \sigma_j \approx 0.14 g^4$ (cf. Ref. [14]).

The cross section is also found to be approximately independent of R (cf. Fig. 5). A similar conclusion was reached in four dimensions in Ref. [5]. On the other hand, the cross section in the strong-coupling limit in four dimensions is found to increase logarithmically with R [24]. Within statistical errors the range in R considered here is not sufficient to rule out such a weak dependence on the radial separation.

Our measurements of the quartet representation ($j = 3/2$) correlators are consistent with the above results. We compare data in the three representations taken from the $T \times R = 5 \times 6$ Wilson loop: energy-density profiles transverse to the flux tube are shown in Fig. 7 and the sum rules Eq. (16) in Fig. 8. Data obtained from larger Wilson loops are consistent with these results, although,
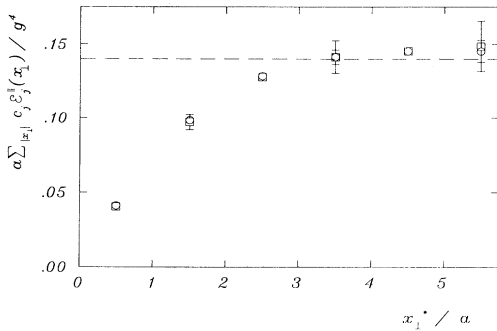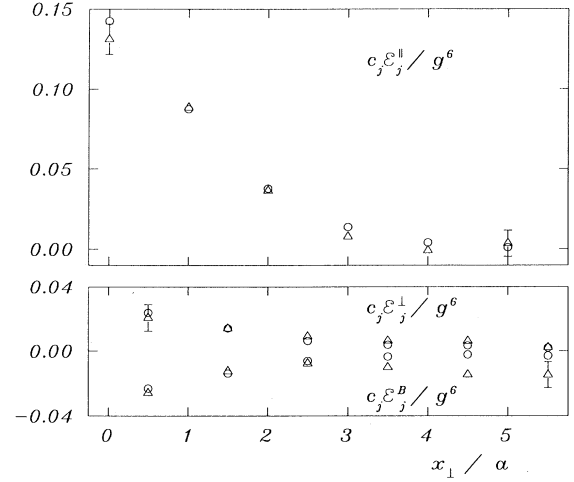

FIG. 7.   Energy-density profile transverse to the plane of the $T \times R = 5 \times 6$ Wilson loop, in the fundamental and quartet representations [$j = 1/2$ ($\circ$), $j = 3/2$ ($\triangle$)].

as mentioned above, the quartet data for larger loops are of poor quality, due to an exponential suppression of the Wilson loop with the Casimir eigenvalue of the representation.

We checked for scaling of the physical flux-tube dimensions by running at $\beta = 14$. The sum rule Eq. (16) for the fundamental representation is compared at the two values of β in Fig. 9. The cutoff $x_\perp^*$ on the sum is expressed here in units of the physical coupling constant g. The data at $\beta = 10$ are for a 6×6 Wilson loop, while the data at $\beta = 14$ are for an 8×8 loop. These Wilson loops have roughly the same dimensions in physical units (T and R measured in units of $1/g^2$).

These results show good evidence for scaling in the energy density and flux-tube cross section (scaling is also observed in our adjoint and quartet representation data). However, the factorization assumed in Eq. (7) breaks down in the $\beta = 14$ data at the largest values of the cut-
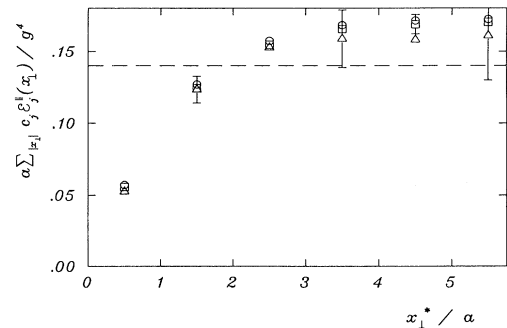

FIG. 6.   Energy sum rule Eq. (16) for the $T \times R = 8 \times 6$ Wilson loop [$j = 1/2$ ($\circ$), $j = 1$ ($\square$)]. The sum in Eq. (16) is evaluated using a variable cutoff $x_\perp^*$. The dashed line shows the scaled string tension $c_j \sigma_j$, estimated to about 5% (cf. Ref. [14]).

FIG. 8.   Energy sum rule Eq. (16) for the $T \times R = 5 \times 6$ Wilson loop, in all three representations [$j = 1/2$ ($\circ$), $j = 1$ ($\square$), $j = 3/2$ ($\triangle$)]. The sum rule improves with increasing T and R (cf. Fig. 6).
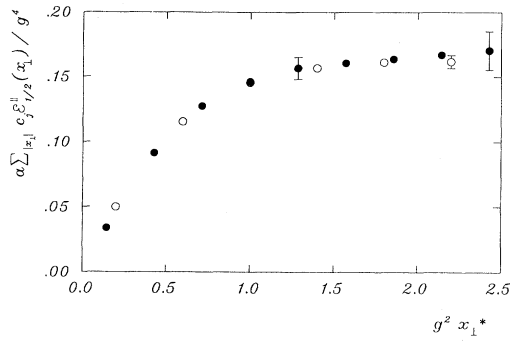
FIG. 9. Scaling of the energy sum rule Eq. (16) for the fundamental representation. The open data points were taken at $\beta = 10$ (for a 6×6 Wilson loop) and the solid points at $\beta = 14$ (for an 8×8 loop). The cutoff $x_\perp^*$ is expressed here in units of the physical coupling constant g.

FIG. 10. T evolution of multiply charged Wilson loops in compact QED$_3$ [$n = 1$ (o), $n = 2$ ($\square$), $n = 3$ ($\triangle$)].

off $x_\perp^*$ shown in Fig. 9 ($x_\perp^* \sim 9.5$ in lattice units, to be compared with $x_R = 16$); the sum is found to diverge linearly with $x_\perp^*$ at large cutoffs. A similar behavior was observed in four-dimensional lattice calculations in Ref. [5], where a correction for this effect was proposed. Nevertheless, scaling of the cross section is clearly supported by data in the region $x_\perp^* \lesssim 1.8/g^2$.

As described in the Introduction, the results of our SU(2) simulation suggest a connection between confinement in QCD and the physics of a dual superconductor. In this connection, we have calculated Wilson loops W_n in compact QED$_3$ for singly and doubly charged sources ($n = 1, 2$):

$$W_n \equiv \mathrm{Re} \prod_{l \in L} (U_l)^n, \qquad (17)$$

where the phase U_l for the link l defines the singly charged representation (i.e., U_l is the phase used to compute the Wilson action). The string tension is expected to scale like the squared charge, as demonstrated by an extension of the Villain approximation used in Ref. [17] to include multiply charged Wilson loops.

Wilson loops and plaquette correlators were measured on a 32^3 lattice at $\beta = 2.4$. More than 10000 sweeps were used for thermalization, and 1000 measurements were made (90 sweeps were taken between measurements). Variance-reduction methods similar to those used in our SU(2) simulations were employed.[2]

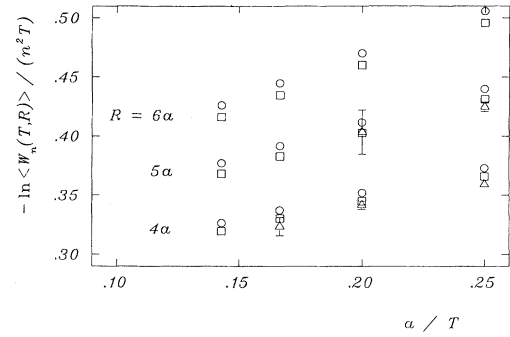Results for the Wilson loops are given in Fig. 10. Some data for the triply charged Wilson loop ($n = 3$) are also

shown (useful measurements of the plaquette correlators for $n = 3$ would require much larger statistics). Estimates of the potential for $n = 1$ obtained from a simple extrapolation of these data are consistent with results presented in graphical form in Ref. [23].

We find that $-\ln \langle W_n(R, T) \rangle / T$, which extrapolates to the potential $V_n(R)$ in the limit $T \to \infty$, scales like n^2 to within about 2% for all T and R that were considered, in good agreement with the expected scaling properties of the string tension. However, the deviation from n^2 scaling is about an order of magnitude larger than the statistical errors in the data. String vibrational modes are known to make a significant contribution to V_1 in the range of R considered here (lattice simulations [23] are in agreement with theoretical expectations [24]). Simple arguments [13] suggest that the vibrational term in V_n may scale like n, which could account for the small deviation from n^2 scaling in the logarithms of the Wilson loops.

The energy sum rule analogous to Eq. (16) for the $T \times R = 5 \times 5$ loop is shown in Fig. 11. The dashed line shows the $n = 1$ string tension taken from Ref. [23]. These results provide the first direct evidence from lattice
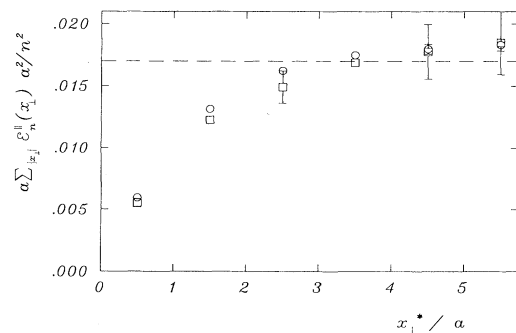

FIG. 11. Energy sum rule Eq. (16) for singly and doubly charged sources in compact QED$_3$, for the $T \times R = 5 \times 5$ Wilson loop [$n = 1$ (o), $n = 2$ ($\square$)]. The dashed line shows the string tension $\sigma_{n=1}$, estimated to about 10% in Ref. [23].

---

[2]The analytical integrals given in Eqs. (8) and (10) are easily adapted to the U(1) theory. The SU(2) link $\mathcal{D}_j[U_l]$ becomes $(U_l)^n$, the Bessel function ratios $I_{2j+1}(x)/I_1(x)$ are replaced by $I_n(x)/I_0(x)$, and det(V) becomes abs(V).

simulations that the flux-tube cross section in compact QED_3 is independent of the source charge as suggested by a simplified flux-tube model [cf. Eq. (1)], given that $\sigma_n \propto n^2$.

IV. SUMMARY

The first direct measurements of the flux-tube cross section as a function of representation in SU(2) lattice-gauge theory were made. We found $\mathcal{A}_j \approx$ const, to within about 10% (a rough estimate of the overall quality of our data) for the three representations $j = 1/2$, 1, and 3/2. Our results are consistent with a connection between the string tension and cross section suggested by a simplified model of flux-tube formation, $\sigma_j = g^2 j(j+1)/(2\mathcal{A}_j)$, given that the string tension scales like the Casimir eigenvalue $j(j + 1)$, as observed in previous lattice studies in both three and four dimensions (and confirmed here up to the quartet representation). We also confirmed several additional qualitative features of the flux-tube picture of color-electric confinement. These results can be used dis-criminate among phenomenological models of the physics underlying confinement. For example, many models in which confinement is due to a bulk property of the QCD vacuum (such as a vacuum pressure) predict a sufficiently rapid increase in $\mathcal{A}_j$ with representation as to be incom-patible with the results obtained from our lattice simu-lations.

We also made flux-tube measurements in compact QED_3, which exhibits electric confinement due to magnetic-monopole condensation. We considered singly and doubly charged Wilson loops. The string tension was found to scale like the squared charge, and the flux-tube cross section was found to be independent of the charge, to a good approximation. The results of our three-dimensional SU(2) and U(1) simulations taken to-gether lend some support, albeit indirectly, to a conjec-ture that the dual-superconductor mechanism underlies confinement in compact gauge theories in both three and four dimensions. This conclusion is also supported by the results of a recent study of dual Abrikosov vortices in an Abelian projection of SU(2) lattice-gauge theory in four dimensions [25]. Flux-tube measurements in four-dimensional SU(2) gauge theory similar to those reported here should be made in order to further explore this pos-sibility.

ACKNOWLEDGMENTS

* Permanent address.

[1] See, for example, P. Hasenfratz and J. Kuti, Phys. Rep. **40C**, 75 (1978).

[2] M. Fukugita and T. Niuya, Phys. Lett. **132B**, 374 (1983).

[3] J. W. Flower and S. W. Otto, Phys. Lett. **160B**, 128 (1985).

[4] R. Sommer, Nucl. Phys. **B291**, 673 (1986); **B306**, 180 (1988).

[5] R. W. Haymaker and J. Wosiek, Phys. Rev. D **36**, 3297 (1987); Acta Phys. Pol. B **21**, 403 (1990); Phys. Rev. D **43**, 2676 (1991).

[6] R. W. Haymaker et al., in *Lattice '89*, Proceedings of the International Symposium, Capri, Italy, 1989, edited by R. Petronzio et al. [Nucl. Phys. B (Proc. Suppl.) **17**, 558 (1990)]; in *Lattice '90*, Proceedings of the International Symposium, Tallahassee, Florida, edited by U.M. Heller, A.D. Kennedy, and S. Sanielevici [ibid. **20**, 207 (1990)].

[7] A. Di Giacomo, M. Maggiore, and S. Olejnik, Phys. Lett. B **236**, 199 (1990).

[8] D. G. Caldi and T. Sterling, Phys. Rev. Lett. **60**, 2454 (1988); Phys. Rev. D **40**, 3447 (1989).

[9] A. Chodos, R. L. Jaffe, K. Johnson, C. B. Thorn, and V. F. Weisskopf, Phys. Rev. D **9**, 3471 (1974).

[10] See, for example, J. Kogut and L. Susskind, Phys. Rev. D **9**, 3501 (1974); C. G. Callan, R. F. Dashen, and D. G. Gross, ibid. **19**, 1826 (1979); H. Pagels and E. Tomboulis, Nucl. Phys. **B143**, 485 (1978); S. L. Adler and T. Piran, Rev. Mod. Phys. **56**, 1 (1984); R. R. Mendel and H. D. Trottier, Phys. Rev. D **40**, 3708 (1989).

[11] See, for example, R. Friedberg and T. D. Lee, Phys. Rev. D **16**, 1096 (1977); T. H. Hansson, K. Johnson, and C. Peterson, ibid. **26**, 2069 (1982).

[12] C. Bernard, Phys. Lett. **108B**, 431 (1982); Nucl. Phys. **B219**, 341 (1983); J. Ambjørn, P. Olesen, and C. Peter-son, ibid. **B240**, 189 (1984); C. Michael, ibid. **B259**, 58 (1985); L. A. Griffiths, C. Michael, and P. Rakow, Phys. Lett. **150B**, 196 (1985); N. A. Campbell, I. H. Jorysz, and C. Michael, ibid. **167B**, 91 (1986).

[13] J. Ambjørn, P. Olesen, and C. Peterson, Nucl. Phys. **B240**, 533 (1984).

[14] R. D. Mawhinney, Phys. Rev. D **41**, 3209 (1990).

[15] See, for example, H. B. Nielsen and P. Olesen, Nucl. Phys. **B61**, 45 (1973).

[16] A. M. Polyakov, Nucl. Phys. **B120**, 429 (1977).

[17] T. Banks, R. Myerson, and J. Kogut, Nucl. Phys. **B129**, 493 (1977).

[18] G. 't Hooft, in *High Energy Physics*, edited by A. Zichichi (Editrice Compositori, Bologna, 1976); S. Mandelstam, Phys. Rep. **23C**, 245 (1976).

[19] G. Parisi, R. Petronzio, and F. Rapuano, Phys. Lett. **128B**, 418 (1983).

[20] C. Michael, Nucl. Phys. **B259**, 58 (1985).

[21] See, for example, K. Redlich and H. Satz, Phys. Lett. B **213**, 191 (1988).

[22] C. Michael, Nucl. Phys. **B280** [FS18], 13 (1987).

[23] A high-statistics study of the $n = 1$ potential was made by R. J. Wensley and J. D. Stack, Phys. Rev. Lett. **63**, 1764 (1989). See also A. Irbäck and C. Peterson, Phys.

Rev. D **36**, 3804 (1987).

[24] M. Lüscher, G. Münster, and P. Weisz, Nucl. Phys. **B180**, 1 (1981); **B180**, 317 (1981).

[25] V. Singh, D. Browne, and R. W. Haymaker, Phys. Lett. B **306**, 115 (1993). See also P. Cea and L. Cosmai, BARI Report No. TH 110/92 (unpublished), for an investigation of the dual Meissner effect.